bioRxiv preprint doi: https://doi.org/10.1101/2021.07.15.452420; this version posted August 2, 2021. The copyright holder for this preprint (which was not certified by peer review) is the author/funder, who has granted bioRxiv a license to display the preprint in perpetuity. It is made available under aCC-BY-NC-ND 4.0 International license.

Title: Induced Membrane Curvature Bypasses Clathrin's Essential Endocytic Function

Authors: Robert C Cail[1], Cyna R Shirazinejad[1], and David G Drubin[1,2] *

Affiliations:

[1]Biophysics Graduate Group, University of California Berkeley; Berkeley, CA, 94720-3202, USA.

[2]Department of Molecular and Cell Biology, University of California Berkeley; Berkeley, CA, 94720-3202, USA.

*Corresponding author. Email: drubin@berkeley.edu

Abstract: During clathrin-mediated endocytosis (CME), flat plasma membrane is rapidly remodeled to produce a nanometer-scale spherical vesicle. The mechanisms underlying this shape change are not known, but it has been hypothesized that the clathrin coat stabilizes membrane curvature. Here, we used nanopatterning to produce glass-like substrates with U-shaped features mimicking membrane shapes induced by fibrillar materials such as collagen. These substrates bend the ventral plasma membranes of cells grown on them into shapes characteristic of the energetically-unfavorable U-shaped intermediate stage of CME. This induced plasma membrane curvature recruits the endocytic machinery and promotes productive endocytosis. Curvature-based localization of the endocytic machinery is unaffected by clathrin disruption, and induced curvature partially bypasses clathrin's role in cargo uptake, supporting the conclusion that clathrin's essential endocytic function is to stabilize membrane curvature.

bioRxiv preprint doi: https://doi.org/10.1101/2021.07.15.452420; this version posted August 2, 2021. The copyright holder for this preprint (which was not certified by peer review) is the author/funder, who has granted bioRxiv a license to display the preprint in perpetuity. It is made available under aCC-BY-NC-ND 4.0 International license.

Main Text

Introduction

Cells grow and migrate in complex 3D environments, wherein nanoscale membrane bending is induced by both external environmental factors and intrinsic cellular processes: constraints outside the cell, such as the extracellular matrix (ECM) and cell-cell junctions, force the cell to adopt particular geometries, and intracellular processes like endocytic vesicle formation reshape the membrane from within[1-3]. Clathrin-mediated endocytosis (CME) is a constitutive membrane-bending process that regulates a wide array of cellular functions including cell signaling, adhesion, and migration[4-6]. To generate vesicles, CME first bends the plasma membrane into a clathrin-coated pit (CCP), at which adaptor proteins such as AP2 bind to cargoes and to curvature-generating coat proteins, creating a spherical vesicle that buds into the cell[7,8]. CCPs localize preferentially to sites of nanoscale curvature in cultured cells[9,10], suggesting that induced plasma membrane geometry may play a physiological role in CCP nucleation and dynamics.

Clathrin is essential for productive CME; upon clathrin disruption through siRNA or chemical inhibition, CCPs stall as protein aggregates with shallow curvature[11,12]. However, clathrin can adopt distinct functional conformations including the spherical cage, flat plaque, and tubular lattice[10,13,14]. This conformational flexibility and variability have led to debate about clathrin's activity during CME: what role does clathrin play in membrane budding, given its affinity for membranes of different curvatures? How does the 3-dimensional structure of the cellular environment, which alters membrane geometry, influence CCP formation and kinetics? Answering these questions promises to provide new insights into how productive CCPs are

bioRxiv preprint doi: https://doi.org/10.1101/2021.07.15.452420; this version posted August 2, 2021. The copyright holder for this preprint (which was not certified by peer review) is the author/funder, who has granted bioRxiv a license to display the preprint in perpetuity. It is made available under aCC-BY-NC-ND 4.0 International license.

formed, and into CME's membrane curvature-generating mechanism. By creating nanofabricated ridges that induce a range of nanoscale membrane curvatures by mimicking ECM fibers across the ventral cell membrane, we set out to answer these questions.

Ormocomp nanoridges induce membrane curvature and recruit the endocytic machinery

To induce membrane curvature across nanometer-range size scales, we applied a low-cost, high-throughput nanofabrication method termed UV-Nanoimprint Lithography (UV-NIL)[15] (Fig 1A). We selected the organic/inorganic hybrid material Ormocomp as our substrate because of the near-exact match of its refractive index to that of borosilicate glass, allowing us to conduct Total Internal Reflection Fluorescence (TIRF) microscopy, a standard imaging method in the CME field[16]. To produce substrates through UV-NIL, we first created a mold through electron-beam lithography and reactive-ion etching on a silicon wafer[17] (Supplementary Figure 1). This mold features mm-long, cylindrical invaginations spaced at a pitch of 2 μm, with widths of 75, 120, 200, 300, 500, and 1000 nm (Fig 1B). The depth of an invagination varies from 200 to 300 nm. This mold served as the basis for Ormocomp substrate production. The resulting Ormocomp substrates bear the inverse geometry of the mold and therefore have cylindrical protrusions, which we term nanoridges (Fig 1B).

Upon exposure to intense UV irradiation, Ormocomp polymerizes through polyacrylate chemistry[18]. Ormocomp substrate manufacturing requires only ~15 minutes per substrate, allowing for replicated experiments and wider screening of conditions than is possible with slower nanofabrication processes.

To determine how the nanoridges affect plasma membrane shape, we seeded MDA-MB-231 cells on nanoridge substrates and performed thin-section TEM of substrate-grown cells.

bioRxiv preprint doi: https://doi.org/10.1101/2021.07.15.452420; this version posted August 2, 2021. The copyright holder for this preprint (which was not certified by peer review) is the author/funder, who has granted bioRxiv a license to display the preprint in perpetuity. It is made available under aCC-BY-NC-ND 4.0 International license.

Electron micrographs revealed that the plasma membrane bends around nanoridges of different diameters (Fig 1C). By measuring the diameter of multiple ridge-membrane interfaces across >3 cells per ridge size, we found that the nanoridges induce consistent membrane diameter as a function of ridge size (Fig 1D). The smallest nanoridge, 75 nanometers, induced a membrane diameter of ~142 nm, approximately 50% larger than the diameter of a fully-formed vesicle, with a linear increase up to the 500 nm ridge, which induced ~650 nm diameter curvature. The shape of the membrane bent around nanoridges was similar to the shapes seen in MDA-MB-231 cell membranes wrapped around collagen fibers, which are known to induce clathrin structures known as Tubular Clathrin/AP2 Lattices (TCALs)[10]. When cells expressing RFP-tagged AP2 (AP2-RFP), an early-arriving CME protein, were grown on the nanoridges, there was a striking localization of AP2-RFP on the ridge (Fig 1E). Thus, Ormocomp nanoridges provide a robust method to create regular, reproducible membrane curvature and to de-couple curvature generation from cell-intrinsic processes such as vesicle formation.

To determine the effect of the diameter of induced membrane curvature on the endocytic machinery, we seeded MDA-MB-231 cells, genome-edited to express fluorescent fusion proteins under endogenous regulatory control[19], on nanoridge substrates and imaged them on a TIRF microscope (Fig 2). Imaging of plasma membrane markers showed that the entirety of the ventral plasma membrane is illuminated by the TIRF microscope (Fig 2A, Supplementary Figure 2). The endocytic proteins demonstrated a striking preference for the higher-curvature ridges (e.g., 75, 120, and 200 nm) (Fig 2B-C), as reported previously for cells grown on quartz substrates[9]. This observation was true of early-arriving endocytic proteins AP2 and clathrin light chain A (Fig 2B), as well as the intermediate curvature-generating protein epsin1 and late-peaking scission GTPase

bioRxiv preprint doi: https://doi.org/10.1101/2021.07.15.452420; this version posted August 2, 2021. The copyright holder for this preprint (which was not certified by peer review) is the author/funder, who has granted bioRxiv a license to display the preprint in perpetuity. It is made available under aCC-BY-NC-ND 4.0 International license.

dynamin2[20,21] (Fig 2C). The plasma membrane protein caveolin-1, which is not a component of CME sites[22], demonstrated no preferred binding to membranes of high curvature (Fig 2D).

To quantify the enrichment of endocytic sites on nanoridges with high curvature, we developed automated image processing tools. Using the bright field image of a cell on a substrate, we employed a line detection algorithm to create a mask that discriminates between on-and-off ridge sections of the cell[23]. We next employed a Differences-of-Gaussians (DoG) algorithm to detect and localize fluorescent puncta[24]. We corrected for increased cell membrane presence on nano-ridges by measuring the on-ridge increase in fluorescence of cell membrane markers BFP-Caax and CellMask Orange, which were in good agreement (Supplementary Figure 2). By measuring the relative abundance of endocytic proteins on the ridge vs flat membrane and dividing by the corrected area of the mask, we determined an enrichment score, which is a relative increase in likelihood of endocytic protein localization as a function of curvature.

The enrichment score demonstrates the strong preference of the endocytic machinery for regions of high plasma membrane curvature (Fig 2E). At the 75-nanometer ridge, AP2-RFP shows a nearly 4-fold increase in puncta localization relative to flat membranes. Epsin1-GFP and dynamin2-GFP both show greater than a 4-fold enrichment. Swapping the fluorophores on AP2 and dynamin2 to GFP and RFP, respectively, resulted in little difference in enrichment (Supplemental Figure 2). These enrichments decrease with increasing diameter, until at the 500-nm ridge there is essentially no detectable enrichment. Clathrin light chain A, in contrast with other endocytic proteins, demonstrates a >3-fold enrichment at the smallest substrate size but precipitously decreases its enrichment as ridge size increases. This reduced enrichment may be because of the presence of clathrin at other trafficking events within the cell body such as

bioRxiv preprint doi: https://doi.org/10.1101/2021.07.15.452420; this version posted August 2, 2021. The copyright holder for this preprint (which was not certified by peer review) is the author/funder, who has granted bioRxiv a license to display the preprint in perpetuity. It is made available under aCC-BY-NC-ND 4.0 International license.

endosomes and the *trans*-Golgi network[25]. These data demonstrate that CME proteins robustly reorganize across the cell in response to induced membrane curvature, with a strong preferential localization at highest induced positive curvature.

Endocytic localizations on nanoridges are sites of *bona fide* CME

We next wondered whether the puncta of endocytic proteins present on curved membranes above nanoridges represent productive CCPs, TCALs, or ectopic protein localization (Fig 3). The ability to perform highly-sensitive TIRF imaging on nanoridge substrates allowed for precise quantitative analysis of fluorophore signal. To determine whether induced curvature promotes formation of productive endocytic sites, we imaged double-genome-edited MDA-MB-231 cells expressing AP2-TagRFP2 (herein called AP2RFP) and dynamin2-EGFP (herein DNM2GFP) at 0.5 Hertz on a range of ridge sizes. Kymographs and montages from two-color movies on flat Ormocomp substrates demonstrated the characteristic track of AP2RFP fluorescence accompanied by a burst of DNM2GFP fluorescence at the end of each AP2RFP track, a hallmark of productive endocytosis[19,26] (Fig 3A-B). Kymographs and montages from 75-, 120-, and 200-nanometer nano-ridges show the same stereotypical endocytic site behavior, indicating that the puncta present on nanoridges are productive CCPs (Fig 3A-B).

By using an established method of endocytic site detection and tracking, we measured the activity of the presumed CCPs over time in AP2RFP and DNM2GFP double-tagged cells[26]. After event detection followed by binning to select for endocytic sites on induced curvature, we applied lifetime, MSD, and colocalization criteria according to previously published standards to select for valid CCPs[19,26-28]. The lifetime of AP2 on flat substrates was 50.9+/-28s, similar to previously reported values for authentic CME sites on glass[19] (Fig 3C). Endocytic sites on

bioRxiv preprint doi: https://doi.org/10.1101/2021.07.15.452420; this version posted August 2, 2021. The copyright holder for this preprint (which was not certified by peer review) is the author/funder, who has granted bioRxiv a license to display the preprint in perpetuity. It is made available under aCC-BY-NC-ND 4.0 International license.

substrates with induced curvature followed the same pattern of AP2 increase followed by a dynamin2 peak, which marks productive vesicle scission, albeit with increased lifetimes of 58.4 +/- 30s for 75 nm ridges, 54.8 +/- 28 s for 120 nm ridges, and 53.5 +/- 29 for 200 nm ridges (Fig 3C-D). At diameters >200 nm, endocytic dynamics were unchanged by nanoridges (Supplementary Figure 3). This lifetime increase on smaller-diameter nanoridges is consistent with the finding that AP2 sites on collagen fibers have longer lifetimes than adjacent, non-collagen CCPs[10]. Nanoridge-associated CCPs demonstrated increased spatial displacement during the last ten-second intervals of their lifetimes relative to CCPs budded from flat membranes (Fig 3E). The nanoridges did not change the percentages of transient, broken, incomplete, or persistent CCPs (Supplementary Figure 3).

In several cases of thin-section TEM we found CME vesicles budding from the side of a nano-ridge, as indicated by the spiked clathrin coat around the forming vesicle[29] (Fig 3F). We also found small, spiked coats on the tops of some ridges, suggesting that this is where the endocytic sites are initiated. These observations, combined with the increased displacement of nanoridge-CCPs before scission, lead us to theorize that endocytic sites preferentially form on sites of high positive curvature, then migrate from the top of the ridge to its side as the pit transitions to maturity and buds into the cell. The bulk rate of endocytosis, as measured by uptake of endocytic cargo transferrin tagged with Alexa-Fluor 647 (tfn-AF647), is not changed by the size of nanoridge[30] (Supplementary Figure 3).

TEM imaging of the 1000-nanometer substrate revealed a flat top with curved sides (Fig 1B); cells grown on this size of ridge bear membrane curvature along the side of the ridge and flat membrane along the top of the ridge (Supplementary Figure 4). The diameter of the

bioRxiv preprint doi: https://doi.org/10.1101/2021.07.15.452420; this version posted August 2, 2021. The copyright holder for this preprint (which was not certified by peer review) is the author/funder, who has granted bioRxiv a license to display the preprint in perpetuity. It is made available under aCC-BY-NC-ND 4.0 International license.

approximate semi-circle on this curved edge of the ridge is ~210 nanometers, similar to that of the 120-nm nanoridge. Consistent with the conclusion that substrate-induced membrane curvature recruits the endocytic machinery, AP2RFP preferentially appears at the edges of the 1000-nm ridges. Indeed, a CCP can be seen by TEM protruding from the high-curvature edge.

Induced curvature rescues endocytic protein recruitment upon clathrin knockdown

We hypothesized that the essential function of clathrin during CME might be to stabilize membrane curvature, and therefore that induced membrane curvature might bypass clathrin function (Fig 4A). Upon siRNA treatment, clathrin heavy chain (*CLTC*) expression was reduced by approximately 95%, as measured by western blot (Fig 4B). Previously, it was established that CME in mammalian cells is inhibited when clathrin is knocked down[31,32], leading to unstable nascent endocytic sites that stall as flat patches. Consistently, compared to sites seen in cells treated with control siRNA, clathrin knockdown on flat substrates leads to dimmer AP2RFP sites with markedly reduced DNM2GFP overlap, indicating that true endocytic sites are not formed (Fig 4C).

However, when clathrin knockdown cells were grown on nanoridges, there was a striking increase in AP2RFP intensity and apparent site size, and robust enrichment of dnm2GFP puncta at the sites of highest curvature was observed (Fig 4D). Thin-section TEM imaging revealed that the diameter of the membrane on nanoridges was unaffected by clathrin knockdown (Suppplementary Figure 5). The enrichment score for AP2RFP and DNM2GFP was unchanged by clathrin siRNA, indicating that these early- and late-arriving CME proteins localize to sites of induced membrane curvature independent of clathrin (Fig 4E).

bioRxiv preprint doi: https://doi.org/10.1101/2021.07.15.452420; this version posted August 2, 2021. The copyright holder for this preprint (which was not certified by peer review) is the author/funder, who has granted bioRxiv a license to display the preprint in perpetuity. It is made available under aCC-BY-NC-ND 4.0 International license.

To test whether formation of curvature-dependent CME sites requires the adaptor protein AP2, we knocked down AP2 expression by siRNA and imaged cells on flat and curved substrates. Upon siRNA treatment, AP2 expression was depleted by >90%, as demonstrated by western blot and by a decrease in AP2 fluorescence in AP2RFP-tagged cells (Fig 4B). AP2 disruption leads to a marked decrease in CLTARFP and DNM2GFP puncta that is not rescued by induced curvature (Fig 4 F-G). AP2-depleted cells on a flat substrate showed 3-fold decreased density of DNM2GFP puncta, and 2-fold decreased density of CLTARFP puncta (Fig 4H). Despite the diameter of induced membrane curvature being unchanged by AP2 siRNA, the enrichment score for CLTARFP decreased significantly upon AP2 knockdown, from approximately 2.2 to 1.1 on 75nm substrates; this decrease in enrichment score is present across substrate sizes, indicating that clathrin is curvature-insensitive after AP2 disruption (Fig 4I). Cells treated with siRNA were illuminated to a depth of approximately 400 nanometers to ensure visualization of the entire ventral side of the cell, leading to an increase in visualization of endosomal or *trans*-Golgi associated CLTARFP puncta, which accounts for the apparent decrease in control-cell CLTARFP enrichment.

DNM2GFP puncta, however, were still 2-fold enriched on sites of high curvature, which is more modestly than in control cells (Fig 4I). This enrichment may be due to some innate curvature preference for dynamin2, or it may be due to dynamin2's roles in other endocytic pathways, which may be curvature-sensitive[33]. These data indicate that curvature-induced endocytic sites depend on an AP2 function to precede endocytic patch stabilization, consistent with previous results[10,31].

bioRxiv preprint doi: https://doi.org/10.1101/2021.07.15.452420; this version posted August 2, 2021. The copyright holder for this preprint (which was not certified by peer review) is the author/funder, who has granted bioRxiv a license to display the preprint in perpetuity. It is made available under aCC-BY-NC-ND 4.0 International license.

Endocytic sites on curved substrates turn over and take up receptors despite clathrin disruption

Once we established that AP2 and dynamin2 localization in clathrin knockdown cells could be rescued by induced membrane curvature, we wondered whether these rescued sites turn over and take up cargo without the clathrin coat. To determine the kinetic profile for these sites over time, we recorded time-lapse TIRF microscopy of AP2/dynamin2 double-labeled cells after clathrin knockdown and tracked endocytic sites over time. We found that for cells treated with control siRNA, the sites of AP2/dynamin2 colocalization appeared as canonical endocytic sites, with a gradual increase in AP2 accompanied by a burst of dynamin2 to indicate scission (Fig 5A). Upon clathrin knockdown on flat substrates, the AP2 puncta were dimmer, small and unstable, with reduced dynamin2 co-localization. However, with substrate-stabilized 75 nm membrane curvature, the AP2 puncta became much larger and more stable; additionally, there was a burst of dynamin2 at a late stage of AP2 lifetime, followed by a decrease in AP2 fluorescence signal, hallmarks of CME vesicle scission. We found that the average lifetime of these tracks in clathrin knockdown cells (68+/-33s) was significantly increased over what was observed in control siRNA cells (50+/-26s), indicating that despite the normal appearance of the sites, their turnover is affected by clathrin knockdown (Fig 5B).

After binning the AP2/dynamin2 positive tracks according to lifetime, we found for cells grown on flat substrates that clathrin knockdown results in a decrease to only ~35% fluorescence signal for AP2/dynamin2 tracks relative to control siRNA (Fig 5C, left). The remaining dynamin2 signal showed a nearly symmetrical, noisy distribution over time, rather than a late-peaking recruitment characteristic of cells treated with control siRNA. However, tracks for cells

bioRxiv preprint doi: https://doi.org/10.1101/2021.07.15.452420; this version posted August 2, 2021. The copyright holder for this preprint (which was not certified by peer review) is the author/funder, who has granted bioRxiv a license to display the preprint in perpetuity. It is made available under aCC-BY-NC-ND 4.0 International license.

grown on 75nm substrates demonstrated a rescue of fluorescence intensity to ~70% of control, and the dynamin2 signal demonstrated the late peak characteristic of productive vesicle formation (Fig 5C, right).

Quantification of the overlap between AP2RFP tracks and DNM2GFP tracks on flat substrates versus curved ridges after clathrin knockdown demonstrates a dramatic rescue in overlap between the two fluorophores, from 29% overlap to 52%, matching the overlap with control siRNA (Fig 5D). In contrast, overlap between AP2GFP tracks and CLTARFP tracks was markedly decreased from 51% to 22%, and this decrease in fluorescence overlap is not changed by induced curvature, evidence that the rescue of the endocytic machinery is not provided by residual clathrin heavy chain.

We next sought to determine whether induced membrane curvature could also rescue cargo uptake in clathrin knockdown cells. We performed transferrin uptake assays with Alexa-Fluor 647-labeled transferrin (tfn-AF647). Upon exposure to media containing tfn-AF647, control siRNA-treated cells demonstrated perinuclear puncta of tfn-AF647, visible in X-Z protections (Fig 5E). In contrast, clathrin knockdown cells showed only membrane-associated tfn-AF647, which binds to its receptor but fails to be internalized. Clathrin knockdown cells with 75 nm of induced curvature, however, demonstrated a marked rescue of perinuclear tfn-AF647 puncta, indicating successful uptake of cargo. We measured the mean pixel intensity across control cells to be ~1200+/-500 AU (Fig 5F, example images in Supplemental Figure 5). Clathrin knockdown cells on flat substrate had a mean pixel intensity of 69+/-22AU, while clathrin knockdown cells with 75nm of induced membrane curvature demonstrated a >3-fold increase in mean pixel intensity to 223+/-73 AU. The intensity of curvature-rescued cells is >4-fold weaker

bioRxiv preprint doi: https://doi.org/10.1101/2021.07.15.452420; this version posted August 2, 2021. The copyright holder for this preprint (which was not certified by peer review) is the author/funder, who has granted bioRxiv a license to display the preprint in perpetuity. It is made available under aCC-BY-NC-ND 4.0 International license.

than control cells, which is consistent with 1) exogenous curvature only partially rescuing endocytosis and 2) only ~⅓ of the cell, the ventral membrane contacting nanoridges, having induced membrane curvature. Through TEM imaging of clathrin knockdown cells, we found membrane-enclosed structures that lack a clear clathrin coat and have an elliptical shape, associated with the plasma membrane on induced curvature; these may represent vesicles near the time of scission produced through curvature-induced rescue of clathrin disruption (Supplemental Figure 5).

Finally, to test whether curvature could rescue cargo uptake in the absence of AP2, we repeated the transferrin uptake assay in the context of AP2 knockdown (Supplemental Figure 5). AP2 knockdown leads to membrane-associated tfn-AF647 signal, as the transferrin binds to its receptor on the plasma membrane but cannot cluster or be taken into the cell. AP2-knockdown cells grown on 75-nanometer ridges demonstrated tfn-AF647 evenly on the plasma membrane, and no puncta were visible over the diffuse membrane signal. The average pixel intensity in AP2-knockdown cells was not changed with statistical significance. This result indicates that, within the sensitivity of our experiments, transferrin and/or its receptor itself are not curvature sensitive, and that CME protein preference for high membrane curvature is downstream of AP2 function.

Conclusions

In this study, to gain insights into the feedback between membrane geometry and biochemical activity, we created induced nanoscale curvature in live cells. An attractive hypothesis for how curvature formation is controlled during vesicle formation is that membrane curvature itself acts as a signal to control biochemical reaction rates such as Bin-Amphiphysin-

bioRxiv preprint doi: https://doi.org/10.1101/2021.07.15.452420; this version posted August 2, 2021. The copyright holder for this preprint (which was not certified by peer review) is the author/funder, who has granted bioRxiv a license to display the preprint in perpetuity. It is made available under aCC-BY-NC-ND 4.0 International license.

RVS domain protein recruitment, receptor clustering or lipid phosphatase activity[34,35]. The UV-NIL approach described here, with its ability to precisely control membrane curvature, coupled with quantitative cellular assays, will allow in vivo studies of many other curvature-sensitive proteins to more fully define how 3D nano-environment affects biochemical reaction rates underlying diverse cellular processes[36].

The factors that determine endocytic site localization in vivo are not fully known; while many cell types have pre-determined loci of preferred endocytosis[37,38], it is unclear how 3D, nanoscale context changes endocytic nucleation and stabilization. Our work and previous studies demonstrate that, all else being equal, endocytic site assembly is strongly biased to regions of high membrane curvature, as can be induced by rigid ECM fibers or by actin-based protrusions at adherens junctions, and that this curvature preference influences assembly of the earliest CME proteins, independent of the clathrin coat. This reaction to physical cues is expected to have biologically relevant downstream consequences in regulation of endocytic activity, as in mesenchymal migration or uptake of cadherins during the epithelial-to-mesenchymal transition (EMT)[10,39].

Clathrin's role during CME has been a topic of debate since the discovery through electron microscopy of its heterogeneous conformations on the cell membrane some 40 years ago[40]. One proposed model of endocytic curvature formation is that clathrin acts as a Brownian ratchet, irreversibly stabilizing the curvature generated by thermal fluctuations and membrane-bending proteins[41]. Consistent with this model, we find that nanoscale curvature itself is sufficient to produce vesicular uptake without a clathrin coat. This curvature-induced

bioRxiv preprint doi: https://doi.org/10.1101/2021.07.15.452420; this version posted August 2, 2021. The copyright holder for this preprint (which was not certified by peer review) is the author/funder, who has granted bioRxiv a license to display the preprint in perpetuity. It is made available under aCC-BY-NC-ND 4.0 International license.

endocytosis may be relevant to other forms of cellular uptake such as compensatory endocytosis, where coat proteins might be absent[42].

Curvature-induced CME, and the plasticity of clathrin coat dependence, may also assist in divergent endocytosis such as viral uptake, as viral particles are orders of magnitude stiffer than the human plasma membrane and are often larger than canonical CCP cargoes[43,44]. Upon clathrin disruption through siRNA, there is frequently a reduction—but not complete inhibition—of viral infectivity[45,46]. Our evidence suggests that, by providing the necessary curvature to stabilize nascent AP2/cargo complexes absent clathrin, endocytic vesicle budding is possible with exogenous physical cues alone.

Materials and Methods

Substrate Nanofabrication

Nanoridge substrates were made from Ormocomp (Microresist Technologies) adhered to Fisher #1 25mm coverslips (12-545-86). Coverslips were prepared by cleaning with isopropyl alcohol followed by spin-coating at 2000 RPM for 45 seconds covered with approximately 50 µL of hexamethyldisilazane (Sigma-Aldrich, 440191) and 5-minute curing at 180 degrees. Ormocomp was shaped using a silicon wafer mold, and polymerized by exposure to 110 seconds of UV at 14 mW on OAI Mask Aligner model 204. Silicon molds were made using EBL (Vistec VB300) on ZEP520A resist followed by Inductively-Coupled Plasma Reactive Ion Etching using Sulfur Hexafluoride (2%) and molecular Oxygen (98%) at -150 deg in liquid nitrogen-cooled chambers (Oxford Plasmalab RIE). ZEP520A was removed from silicon using acetone/IPA washes. Hydrophobicity of silicon mold was maintained by gas-phase trichloro-perfluoroctylsilane deposition (Sigma-Aldritch 448931-10G) for 30 minutes in vacuum chamber

bioRxiv preprint doi: https://doi.org/10.1101/2021.07.15.452420; this version posted August 2, 2021. The copyright holder for this preprint (which was not certified by peer review) is the author/funder, who has granted bioRxiv a license to display the preprint in perpetuity. It is made available under aCC-BY-NC-ND 4.0 International license.

followed by curing at 150 deg for 10 minutes. Polymerized Ormocomp substrates were stored at room temp for up to two weeks prior to use, and irradiated with UV light for 12 minutes to sterilize prior to use in cell culture. Ormocomp substrate shape was determined by SEM imaging: Ormocomp was sputter-coated in titanium to a thickness of 1-2 nanometers and imaged on Hitachi S-5000 SEM.

Cell Culture and transfection

MDA-MB-231 cells were genome-edited[19] to express fluorescent fusion proteins. Cells were grown in DMEM/f12 (Life Technologies 10565-018) with 10% (v/v) FBS (Seradigm 89510-186) and Penicillin/Streptomycin (Life Technologies 15140-122) to no more than 20 passages. Cells were plated directly onto sterilized Ormocomp substrates at 70% confluence (approximately 8 x 10^5 cells per well) 18-24 hours prior to experiments or imaging.

Cells were prepared for TEM by fixation in 2% gluteraldehyde in cytoskeleton stabilization buffer (100 mM methyl ester sulfonate, 150 mM NaCl, 5 mM EGTA, 5 mM MgCl2, and 5 mM glucose in ddH2O, pH 6.8), rinsed 3x in PBS pH 7.4, stained in 1% Osmium tetroxide and 1.6% Potassium ferricyanide in PBS pH 7.4, and rinsed 3x in PBS pH 7.4. Cells were dehydrated in 7-minute washes in 30%, 50%, 70%, 95%, 100%, and 100% ice-cold ethanol and infiltrated in epon-araldite resin. Resin was polymerized in a 60-degree oven for 24 hours, then 70 nm sections were cut with an Ultracut E (Leica) and collected onto formvar-coated 50 mesh copper grids. Grids were post-stained with 2% uranyl acetate followed by Reynold's lead citrate for 5 minutes each. Sections were imaged using a Tecnai 12 120kV TEM (FEI) and data recorded using an UltraScan 1000 with Digital Micrograph 3 software (Gatan Inc.). Membrane diameter measurements were made using ImageJ.

bioRxiv preprint doi: https://doi.org/10.1101/2021.07.15.452420; this version posted August 2, 2021. The copyright holder for this preprint (which was not certified by peer review) is the author/funder, who has granted bioRxiv a license to display the preprint in perpetuity. It is made available under aCC-BY-NC-ND 4.0 International license.

BFP-Caax in mammalian expression vector (pTagBFP2-C1), a generous gift from the Michael Rape lab (UC Berkeley), was transfected into cells on Ormocomp substrates at 70% confluence using lipofectamine 3000 (Invitrogen L3000008) according to manufacturer protocols (https://tools.thermofisher.com/content/sfs/manuals/lipofectamine3000_protocol.pdf). Cells were imaged 18-24 hours after transfection. CellMask Orange (Invitrogen C10045) was diluted 1000x in media prior to staining; staining was performed for 10 minutes at 37 degrees, followed by two washes in fresh 37-degree media prior to imaging.

Dharmacon smartpool siRNAs (L-004001-01-0005, L-008170-00-0005, and D-001810-10-05) were used to knockdown Clathrin Heavy Chain or AP2Mu1, or a non-targeting control was used, respectively. Cells were transfected using lipofectamine 3000 according to manufacturer protocols (https://tools.thermofisher.com/content/sfs/manuals/lipofectamine3000_protocol.pdf), using an siRNA final concentration of 20 nM. Cells were incubated for 72 hours post-transfection prior to imaging. 18-24 hours prior to imaging or experiment, cells were split. 50% of cells were seeded on Ormocomp substrates. The remaining cells were re-plated, grown until imaging of Ormocomp substrates, then harvested for western blot analysis to determine knockdown efficiency. For western blots, cells were washed on ice in cold DPBS (Gibco 14190-144), lysed on ice using pre-chilled cell scrapers (Corning 3008) in lysis buffer (150 mM NaCl, 1% NP-40, 50mM Tris pH 8.0, 1x Roche protease inhibitor tablet (11697498001)), with immediate addition of 4x Laemmli buffer and 0.5% (v/v) beta-mercaptoethanol. Samples were thoroughly mixed by scraping tubes along a tube rack, boiled for 5 minutes, then centrifuged at 17,900 x g for 5 min before running at 120V on 10% SDS-polyacrylamide gel. Gels were transferred to nitrocellulose membrane (GE Healthcare

bioRxiv preprint doi: https://doi.org/10.1101/2021.07.15.452420; this version posted August 2, 2021. The copyright holder for this preprint (which was not certified by peer review) is the author/funder, who has granted bioRxiv a license to display the preprint in perpetuity. It is made available under aCC-BY-NC-ND 4.0 International license.

10600006) for 90 minutes at 40V in 4-degree transfer buffer (25 mM Tris base, 192 mM glycine, 20% (v/v) methanol), then blocked for 1 hour at room temperature in 5% milk in TBSt (10 mM Tris, 0.09% (w/v) NaCl, 0.05% (v/v) tween-20, pH 7.5). Membranes were probed with clathrin heavy chain antibody (Abcam ab1679) at 1:500 dilution in TBSt with 5% milk, AP2M1 antibody (Abcam ab75995) at 1:1000 dilution in TBSt with 5% milk, or GAPDH antibody (Abcam ab9485) at 1:2000 dilution in TBSt, all for 1 hour at room temperature, followed by 4 x 10-minute wash in TBSt. Secondary antibodies (LICOR, 926-32213) were blotted at 1:2500 dilution in TBSt for 1 hour at room temperature, followed by 4 x 10-minute wash in TBSt and immediate imaging on LICOR Odyssey CLx.

Transferrin uptake assays were performed by serum-starving cells in DMEM/f12 with 0.5% (w/v) BSA (Sigma Life Sciences A9647) for 30 minutes followed by adding fresh DMEM/f12/ BSA with alexa-fluor 647-labeled transferrin at a concentration of 10 micrograms/milliliter (Jackson Immunoresesarch 009-600-050). Cells were exposed to transferrin for 2 minutes followed by 2 minute chase in fresh DMEM/f12/BSA. Cells were then washed 1x with ice-cold DPBS. Cells were fixed in 4% paraformaldehyde (Electron Microscopy Solutions) in Tris/ potassium chloride cytoskeleton buffer (10mM MES, 150mM NaCl, 5mM EGTA, 5mM glucose, 5mM MgCl2, 0.005% Sodium Azide, pH 6.1) for 20 minutes at room temperature, followed by 3 x 5-minute washes in 50mM ammonium chloride in cytoskeleton buffer, and mounted on microscope slide in fluorescence mounting medium (Vectashield H-2000) and either imaged immediately on a confocal microscope or stored at 4 degrees overnight until confocal imaging.

bioRxiv preprint doi: https://doi.org/10.1101/2021.07.15.452420; this version posted August 2, 2021. The copyright holder for this preprint (which was not certified by peer review) is the author/funder, who has granted bioRxiv a license to display the preprint in perpetuity. It is made available under aCC-BY-NC-ND 4.0 International license.

Microscopy

TIRF microscopy was carried out using a Nikon Eclipse Ti2 TIRF microscope with Hamamatsu Orca 4.0 sCMOS camera operated by Nikon Elements software. The TIRF angle was adjusted to pseudo-TIRF to create an evanescent field of approximately 300 nanometers, extending above the bottom of the pillars to ensure illumination of the membrane on the top of the pillars. Best illumination of the membrane and endocytic fluorophores was generated by aligning the illumination angle parallel to the direction of the nanoridges, as determined empirically.

Confocal microscopy for control siRNA and CLTC knockdown cells was done on a Zeiss LSM 900 with Airyscan 2.0 detection, in 4Y multiplex mode, operated by ZEN Blue software. Entire cell volumes were collected at Nyquist sampling frequency (140 nm per Z-section), and maximum intensity projections were created in ImageJ for analysis. Images were batch-processed by ZEN Blue software for Airyscan reconstructions using filter strength setting of 6.

Confocal microscopy for AP2 knockdown cells and for no-treatment transferrin uptake assays was done on a Nikon Eclipse Ti microscope with Yokogawa spinning disk and Andor EMCCD, operated by Nikon Elements software. Entire cell volumes were collected at Nyquist sampling frequency (200nm per Z-section), and maximum intensity projections were created in ImageJ for analysis.

Computational Analysis

Puncta of endocytic proteins were detected using Trackmate 6.0.3 in Differences-of-Gaussians mode[24]. Nanoridges were detected using custom Python scripts built on the Hough transform in Python package cv2[23]. TIRF videos were analyzed using the MATLAB

bioRxiv preprint doi: https://doi.org/10.1101/2021.07.15.452420; this version posted August 2, 2021. The copyright holder for this preprint (which was not certified by peer review) is the author/funder, who has granted bioRxiv a license to display the preprint in perpetuity. It is made available under aCC-BY-NC-ND 4.0 International license.

cmeAnalysis package[26]. Standard settings for model-based detection, Gaussian fitting, radius of detection, and gap closing were selected. Further postprocessing was completed using custom Python scripts, available at github.com/drubinbarneslab. Valid endocytic sites were selected based on lifetime limits of 18-180 seconds, MSD measurement of 0.02 micron^2, and at least 4 consecutive seconds of dynamin2 detection, as have been previously reported for valid CCPs.

Statistical analyses were conducted either with python packages NumPy, Pandas, SciPy, and Seaborns, or with Prism 9. Graphs were produced with Prism 9.

References

1. Suleiman, H. et al. Nanoscale protein architecture of the kidney glomerular basement membrane. Elife 2, (2013).

2. Liu, Z. et al. Mechanical tugging force regulates the size of cell-cell junctions. doi:10.1073/pnas.0914547107/-/DCSupplemental.

3. Hassinger, J. E., Oster, G., Drubin, D. G. & Rangamani, P. Design principles for robust vesiculation in clathrin-mediated endocytosis. doi:10.1073/pnas.1617705114.

4. Vieira, A. V., Lamaze, C. & Schmid, S. L. Control of EGF Receptor Signaling by Clathrin-Mediated Endocytosis. Science 274 (5295), 2086-2089 (1996).

5. Ezratty, E. J., Bertaux, C., Marcantonio, E. E. & Gundersen, G. G. Clathrin mediates integrin endocytosis for focal adhesion disassembly in migrating cells. J. Cell Biol. 187, 733–747 (2009).

6. Paul, N. R., Jacquemet, G. & Caswell, P. T. Endocytic Trafficking of Integrins in Cell Migration. Curr. Biol. 25, R1092–R1105 (2015).

7. Jackson, L. P. et al. A large-scale conformational change couples membrane recruitment to cargo binding in the AP2 clathrin adaptor complex. Cell 141, 1220–1229 (2010).

bioRxiv preprint doi: https://doi.org/10.1101/2021.07.15.452420; this version posted August 2, 2021. The copyright holder for this preprint (which was not certified by peer review) is the author/funder, who has granted bioRxiv a license to display the preprint in perpetuity. It is made available under aCC-BY-NC-ND 4.0 International license.

8. Haucke, V. & Kozlov, M. M. Membrane remodeling in clathrin-mediated endocytosis. J. Cell Sci. 131, 1–10 (2018).

9. Zhao, W. et al. Nanoscale manipulation of membrane curvature for probing endocytosis in live cells. Nat. Nanotechnol. 12, 750–756 (2017).

10. Elkhatib, N. et al. Tubular clathrin/AP-2 lattices pinch collagen fibers to support 3D cell migration. doi:10.1126/science.aal4713.

11. Hinrichsen, L., Meyerholz, A., Groos, S. & Ungewickell, E. J. Bending a membrane: How clathrin affects budding. Proc. Natl. Acad. Sci. U. S. A. 103, 8715–8720 (2006).

12. Von Kleist, L. et al. Role of the Clathrin Terminal Domain in Regulating Coated Pit Dynamics Revealed by Small Molecule Inhibition. Cell 146, 471–484 (2011).

13. Kovtun, O., Dickson, V. K., Kelly, B. T., Owen, D. J. & Briggs, J. A. G. Architecture of the AP2/clathrin coat on the membranes of clathrin-coated vesicles. Sci. Adv vol. 6 (2020).

14. Leyton-Puig, D. et al. ARTICLE Flat clathrin lattices are dynamic actin-controlled hubs for clathrin-mediated endocytosis and signalling of specific receptors. Nat. Commun. 8, (2017).

15. Bender, M., Otto, M., Hadam, B., Spangenberg, B. & Kurz, H. Multiple imprinting in UV-based nanoimprint lithography: Related material issues. in Microelectronic Engineering vols 61–62 407–413 (2002).

16. Gissibl, T., Wagner, S., Sykora, J., Schmid, M. & Giessen, H. Refractive index measurements of photo-resists for three-dimensional direct laser writing. Opt. Mater. Express 7, 2293 (2017).

17. Fischer, P. B. & Chou, S. Y. Sub-50 nm high aspect-ratio silicon pillars, ridges and trenches fabricated using ultra-high E-beam lithography and RIE. Conf. Solid State Devices Mater. 1414, 443–445 (1992).

bioRxiv preprint doi: https://doi.org/10.1101/2021.07.15.452420; this version posted August 2, 2021. The copyright holder for this preprint (which was not certified by peer review) is the author/funder, who has granted bioRxiv a license to display the preprint in perpetuity. It is made available under aCC-BY-NC-ND 4.0 International license.

18. Nason, C., Roper, T., Hoyle, C. & Pojman, J. A. UV-induced frontal polymerization of multifunctional (meth)acrylates. Macromolecules 38, 5506–5512 (2005).

19. Hong, S. H., Cortesio, C. L. & Drubin, D. G. Machine-Learning-Based Analysis in Genome-Edited Cells Reveals the Efficiency of Clathrin-Mediated Endocytosis. Cell Rep. 12, 2121–2130 (2015).

20. Ford, M. G. J. et al. Curvature of clathrin-coated pits driven by epsin. Nature 419, 361–366 (2002).

21. Grassart, A. et al. Actin and dynamin2 dynamics and interplay during clathrin-mediated endocytosis. J. Cell Biol. 205, 721–735 (2014).

22. Rothberg, K. G. et al. Caveolin, a protein component of caveolae membrane coats. Cell 68, 673–682 (1992).

23. Gollapudi S. (2019) OpenCV with Python. In: Learn Computer Vision Using OpenCV. Apress, Berkeley, CA. https://doi.org/10.1007/978-1-4842-4261-2_2

24. Tinevez, J. Y. et al. TrackMate: An open and extensible platform for single-particle tracking. Methods 115, 80–90 (2017).

25. Stoorvogel, W., Oorschot, V. & Geuze, H. J. A novel class of clathrin-coated vesicles budding from endosomes. J. Cell Biol. 132, 21–33 (1996).

26. Aguet, F., Antonescu, C. N., Mettlen, M., Schmid, S. L. & Danuser, G. Advances in analysis of low signal-to-noise images link dynamin and AP2 to the functions of an endocytic checkpoint. Dev. Cell 26, 279–291 (2013).

27. Doyon, J. B. et al. Rapid and efficient clathrin-mediated endocytosis revealed in genome-edited mammalian cells. Nat. Cell Biol. 13, 331–337 (2011).

bioRxiv preprint doi: https://doi.org/10.1101/2021.07.15.452420; this version posted August 2, 2021. The copyright holder for this preprint (which was not certified by peer review) is the author/funder, who has granted bioRxiv a license to display the preprint in perpetuity. It is made available under aCC-BY-NC-ND 4.0 International license.

28. Pascolutti, R. et al. Molecularly Distinct Clathrin-Coated Pits Differentially Impact EGFR Fate and Signaling. Cell Rep. 27, 3049-3061.e6 (2019).

29. Roth, T. F. & Porter, K. R. Yolk Protein Uptake in the Oocyte of the Mosquito Aedes Aegypti. L. J. Cell Biol. 20, 313–332 (1964).

30. Harding, C., Heuser, J. & Stahl, P. Receptor-mediated endocytosis of transferrin and recycling of the transferrin receptor in rat reticulocytes. J. Cell Biol. 97, 329–339 (1983).

31. Motley, A., Bright, N. A., Seaman, M. N. J. & Robinson, M. S. Clathrin-mediated endocytosis in AP-2-depleted cells. J. Cell Biol. 162, 909–918 (2003).

32. Hinrichsen, L., Harborth, J., Andrees, L., Weber, K. & Ungewickell, E. J. Effect of Clathrin Heavy Chain- and α-Adaptin-specific Small Inhibitory RNAs on Endocytic Accessory Proteins and Receptor Trafficking in HeLa Cells. J. Biol. Chem. 278, 45160–45170 (2003).

33. Henley, J. R., Krueger, E. W. A., Oswald, B. J. & McNiven, M. A. Dynamin-mediated internalization of caveolae. J. Cell Biol. 141, 85–99 (1998).

34. Liu, J., Sun, Y., Drubin, D. G. & Oster, G. F. The mechanochemistry of endocytosis. PLoS Biol. 7, (2009).

35. Daumke, O., Roux, A. & Haucke, V. BAR Domain Scaffolds in Dynamin-Mediated Membrane Fission. Cell 156, 882–892 (2014).

36. McMahon, H. T. & Gallop, J. L. Membrane Curvature and the Mechanisms of Dynamic Cell Membrane Remodelling. Nature 438, 590-596 (2005).

37. Murthy, V. N. & De Camilli, P. Cell biology of the presynaptic terminal. Annu. Rev. Neurosci. 26, 701–728 (2003).

bioRxiv preprint doi: https://doi.org/10.1101/2021.07.15.452420; this version posted August 2, 2021. The copyright holder for this preprint (which was not certified by peer review) is the author/funder, who has granted bioRxiv a license to display the preprint in perpetuity. It is made available under aCC-BY-NC-ND 4.0 International license.

38. Tojima, T., Itofusa, R. & Kamiguchi, H. Asymmetric clathrin-mediated endocytosis drives repulsive growth cone guidance. Neuron 66, 370–377 (2010).

39. Delva, E. & Kowalczyk, A. P. Regulation of cadherin trafficking. Traffic 10, 259–267 (2009).

40. Heuser, J. & Evans, L. Three-dimensional visualization of coated vesicle formation in fibroblasts. J. Cell Biol. 84, 560–583 (1980).

41. Sochacki, K. A. & Taraska, J. W. From Flat to Curved Clathrin: Controlling a Plastic Ratchet. (2018) doi:10.1016/j.tcb.2018.12.002.

42. Sokac, A. M., Co, C., Taunton, J. & Bement, W. Cdc42-dependent actin polymerization during compensatory endocytosis in Xenopus eggs. Nat. Cell Biol. 5, 727–732 (2003).

43. Mateu, M. G. Mechanical properties of viruses analyzed by atomic force microscopy: A virological perspective. Virus Research vol. 168 1–22 (2012).

44. Ehrlich, M. et al. Endocytosis by random initiation and stabilization of clathrin-coated pits. Cell 118, 591–605 (2004).

45. Inoue, Y. et al. Clathrin-Dependent Entry of Severe Acute Respiratory Syndrome Coronavirus into Target Cells Expressing ACE2 with the Cytoplasmic Tail Deleted. J. Virol. 81, 8722–8729 (2007).

46. Sun, X., Yau, V. K., Briggs, B. J. & Whittaker, G. R. Role of clathrin-mediated endocytosis during vesicular stomatitis virus entry into host cells. Virology 338, 53–60 (2005).

Acknowledgments:

We gratefully acknowledge Danielle Jorgens, Reena Zalpuri, and Guangwei Min of the UC Berkeley Electron Microscopy Lab for consultation and assistance in TEM and SEM imaging. Spinning-disk confocal imaging was conducted at the CRL Molecular Imaging Center,

bioRxiv preprint doi: https://doi.org/10.1101/2021.07.15.452420; this version posted August 2, 2021. The copyright holder for this preprint (which was not certified by peer review) is the author/funder, who has granted bioRxiv a license to display the preprint in perpetuity. It is made available under aCC-BY-NC-ND 4.0 International license.

supported by the Gordon and Betty Moore Foundation. We also thank Stefano Cabrini, Scott Dhuey, Giuessepe Calafiore, and Stefano Dallorto of the Lawrence Berkeley Lab Molecular Foundry for assistance in silicon mold EBL/etching and Ormocomp substrate manufacturing, and Paul Lum of the UC Berkeley Biomoleuclar Nanotechnology Center for advice and assistance in Ormocomp lithography. Work at the Molecular Foundry was supported by the Office of Science, Office of Basic Energy Sciences, of the U.S. Department of Energy under Contract No. DE-AC02-05CH11231. We thank James Hurley and Leanna Owen of UC Berkeley and Ross Pedersen of the Carnegie Institute for comments on the manuscript.

Funding: National Institutes of Health grant R35GM118149 (DGD)

Author contributions:

Experiments were conceptualized by RCC and DGD, and carried out by RCC. Data analysis and visualization were done by RCC and CRS. RCC and DGD wrote the manuscript; all authors contributed to editing.

Competing interests: Authors declare no competing interests.

Data and materials availability: All data are available in the main and supplementary figures. Code for analysis can be found at github.com/drubinbarneslab.

Supplementary Materials

Figs. S1 to S5

bioRxiv preprint doi: https://doi.org/10.1101/2021.07.15.452420; this version posted August 2, 2021. The copyright holder for this preprint (which was not certified by peer review) is the author/funder, who has granted bioRxiv a license to display the preprint in perpetuity. It is made available under aCC-BY-NC-ND 4.0 International license.

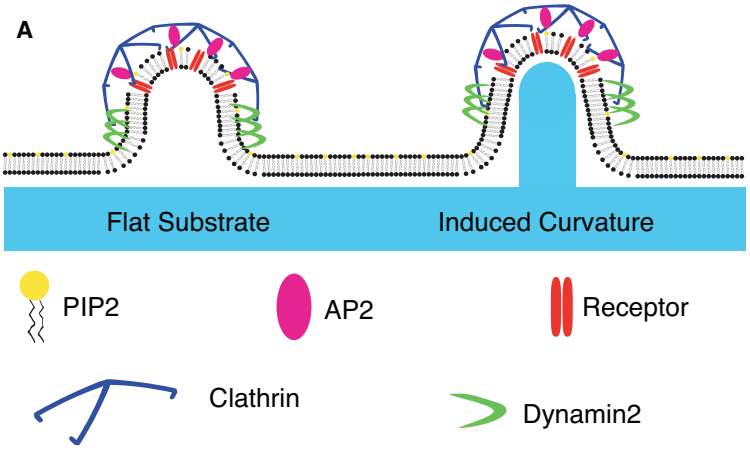

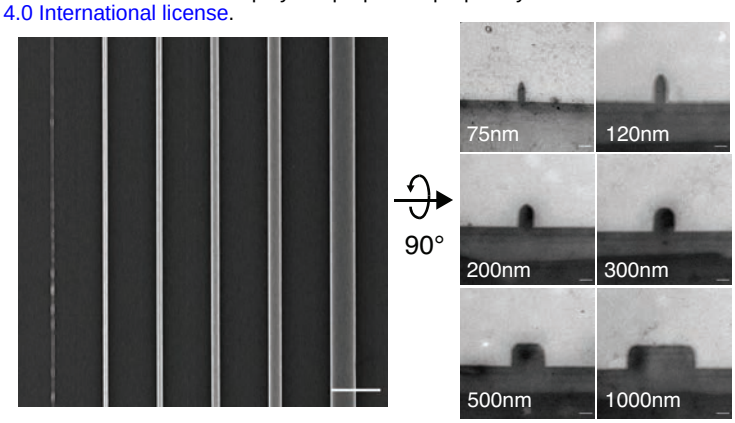

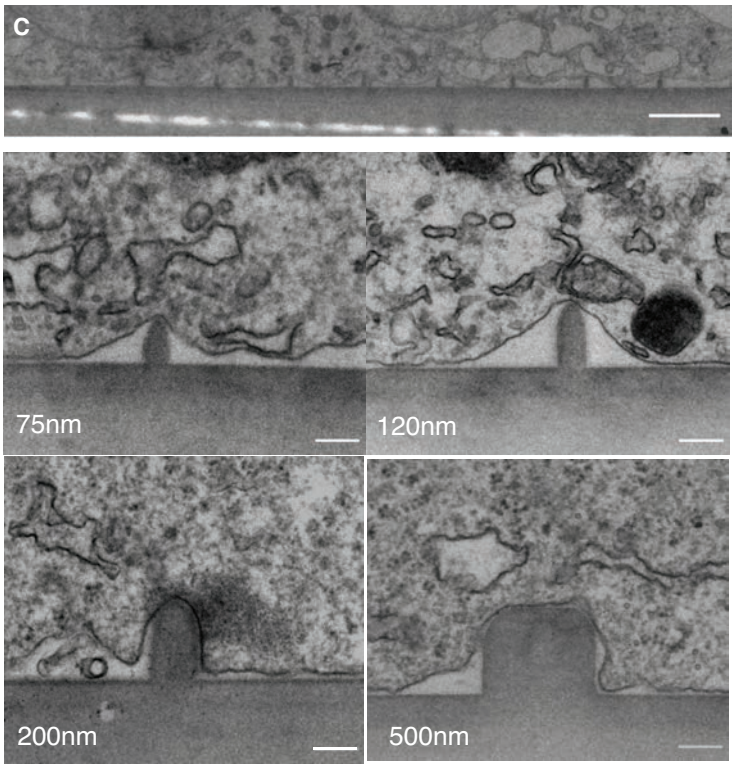

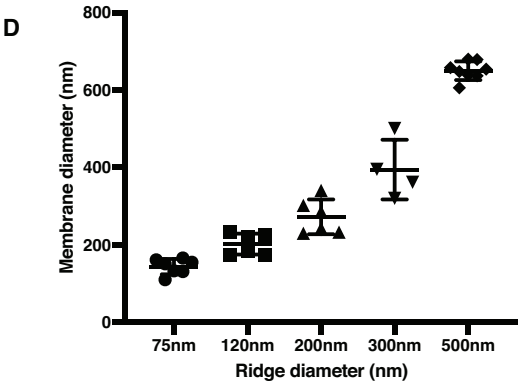

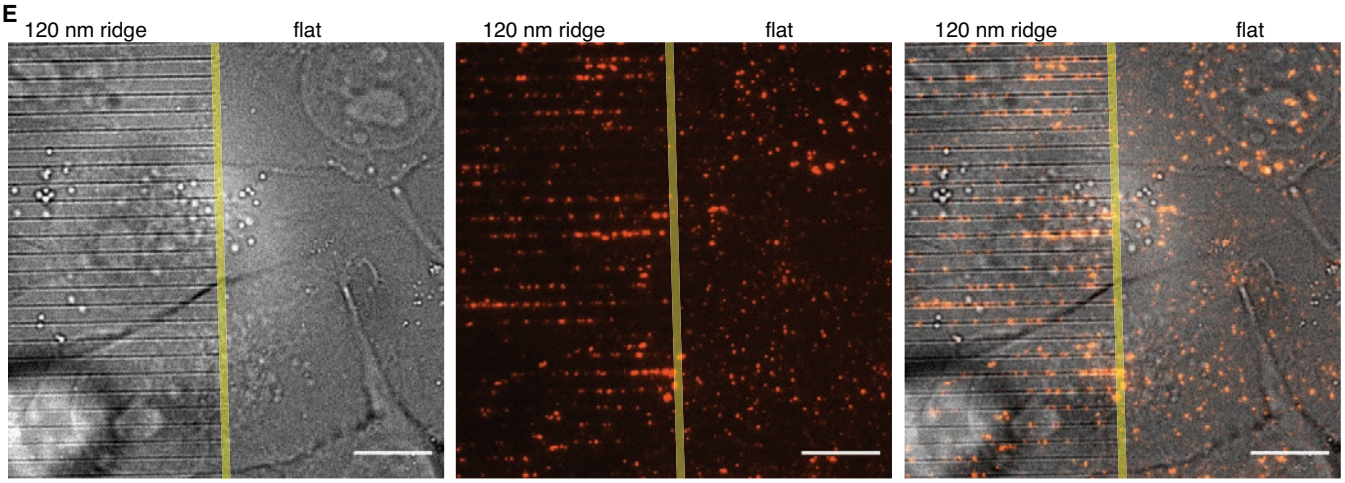

bioRxiv preprint doi: https://doi.org/10.1101/2021.07.15.452420; this version posted August 2, 2021. The copyright holder for this preprint (which was not certified by peer review) is the author/funder, who has granted bioRxiv a license to display the preprint in perpetuity. It is made available under aCC-BY-NC-ND 4.0 International license.

Fig. 1. Ormocomp substrates induce nanometer-scale membrane curvature. (**A**) Induced curvature on the same size order as CCPs may stabilize the energetically-unfavorable U-shaped intermediate state of CME. (**B**) (Left) En-Face SEM of nanoridge substrates showing variable diameter of the ridge (scale bar 2 μM), and (right) thin-section TEM of nanoridges demonstrating the size and shape of nanoridges on which cells grow (scale bar 100 nm). (**C**) Thin-section TEM images of cells grown on nanoridges demonstrates the entire ventral membrane's response to induced curvature (scale bar 2 μM) as well as high-magnification images of cells bent around ridges of varying diameter with induced semi-circular membranes (scale bar 200nm). (**D**) Quantification of membrane diameter induced by nanoridges (Mean ± SD, $n \geq 4$ ridges from $n \geq 3$ cells). (**E**) TIRF/BF microscopy of live MDA-MB-231 cells grown on the edge of a nanoridge section demonstrates AP2 rearrangement in response to ridges (scale bar 10 μM).

bioRxiv preprint doi: https://doi.org/10.1101/2021.07.15.452420; this version posted August 2, 2021. The copyright holder for this preprint (which was not certified by peer review) is the author/funder, who has granted bioRxiv a license to display the preprint in perpetuity. It is made available under aCC-BY-NC-ND 4.0 International license.

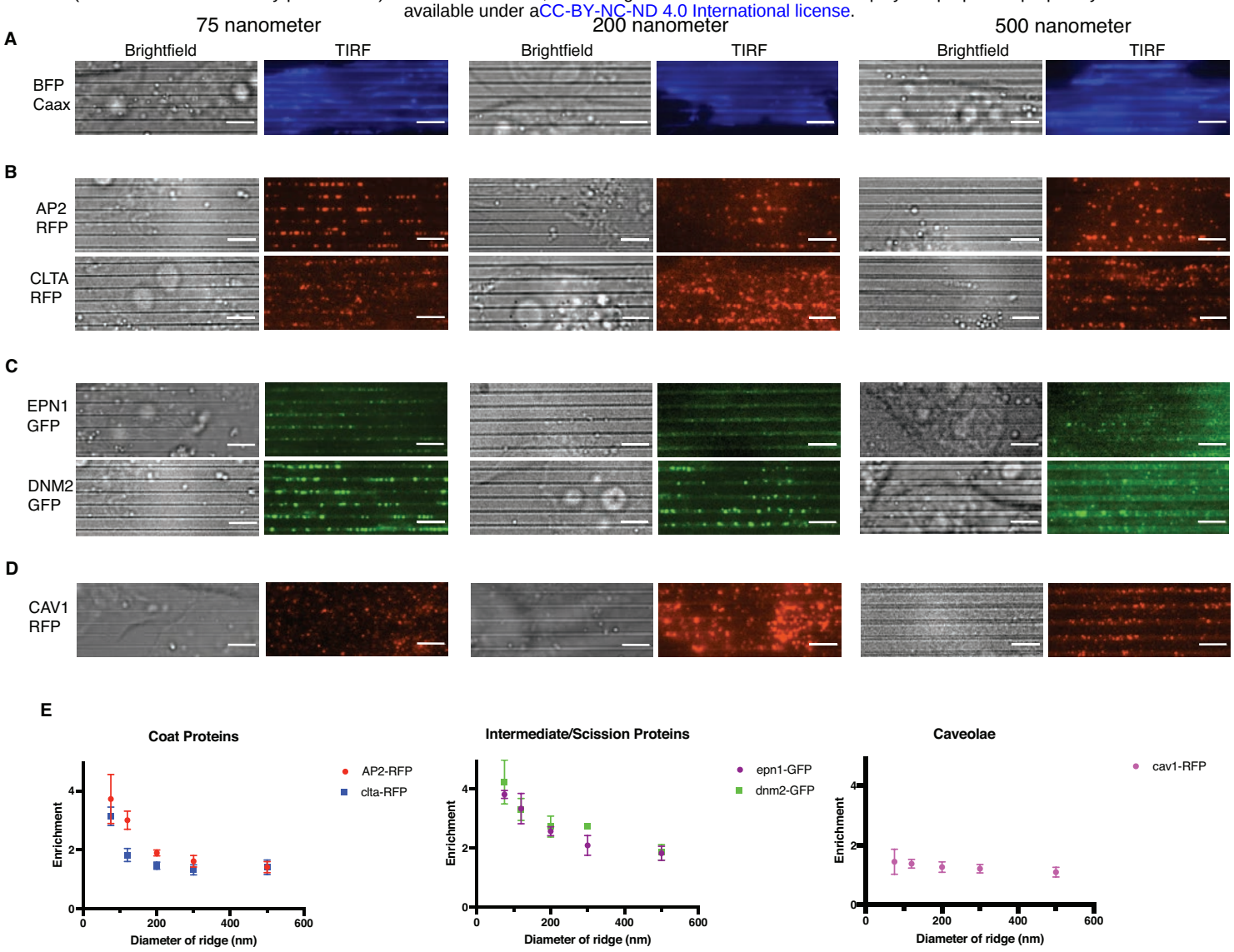

Fig. 2. Proteins from across CME respond to induced curvature as a function of radius. (**A**) TIRF microscopy of cell membrane marker BFP-Caax demonstrating even illumination across the ventral cell body. (**B-D)** Survey of endocytic proteins from across CME and caveolar endocytosis, imaged by TIRF microscopy, demonstrating strong CCP response to smallest-diameter curvature with weaker response to larger diameters. Caveolin-RFP shows no curvature preference (scale bars 4 μM). (**E**) Quantification of enrichment of endocytic proteins surveyed on ridges as a function of ridge diameter (Mean ± SD, $n \geq 5$ cells per condition).

bioRxiv preprint doi: https://doi.org/10.1101/2021.07.15.452420; this version posted August 2, 2021. The copyright holder for this preprint (which was not certified by peer review) is the author/funder, who has granted bioRxiv a license to display the preprint in perpetuity. It is made available under a CC-BY-NC-ND 4.0 International license.

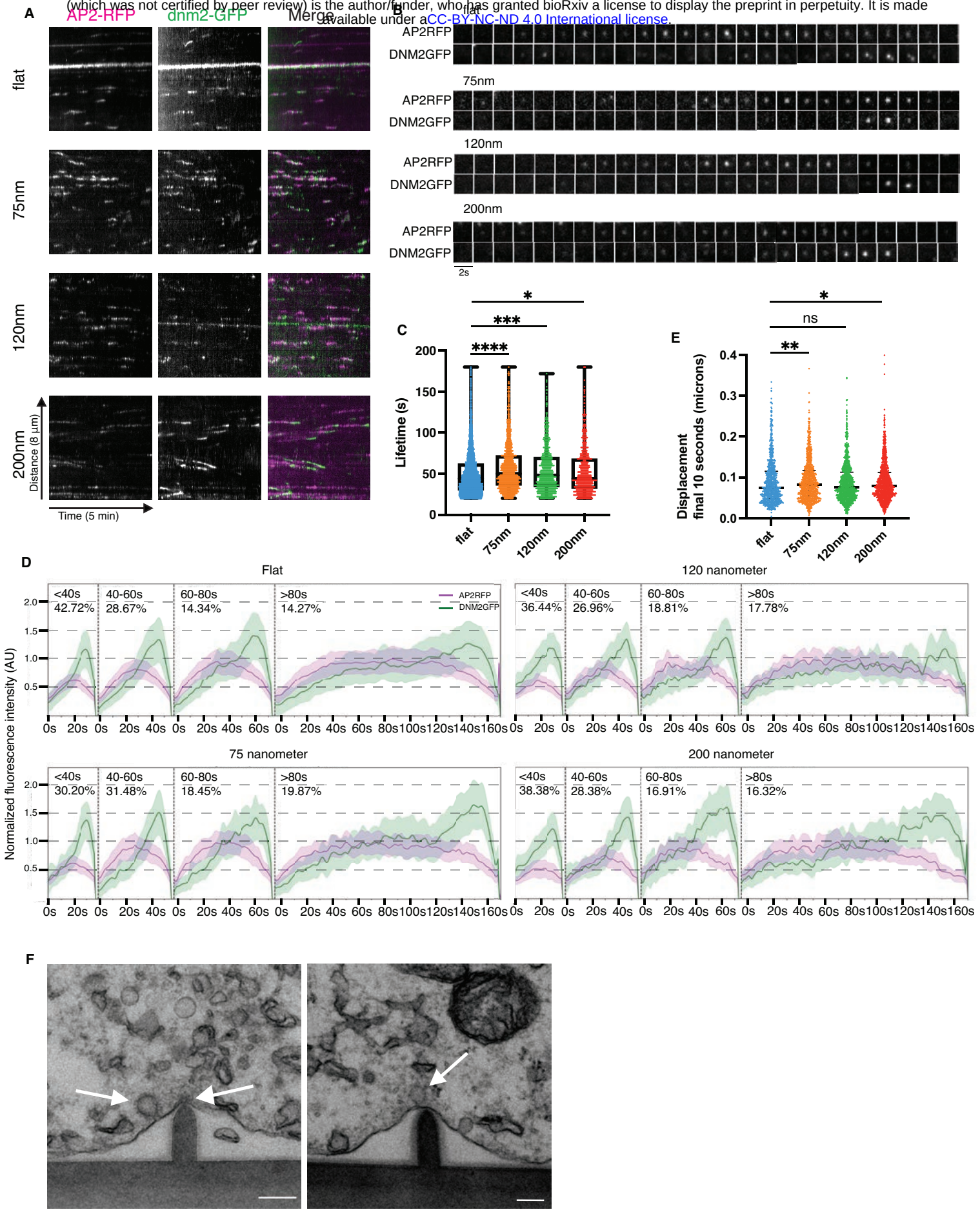

bioRxiv preprint doi: https://doi.org/10.1101/2021.07.15.452420; this version posted August 2, 2021. The copyright holder for this preprint (which was not certified by peer review) is the author/funder, who has granted bioRxiv a license to display the preprint in perpetuity. It is made available under aCC-BY-NC-ND 4.0 International license.

Fig. 3. Endocytic protein localizations on nanoridges are bona fide CCPs with distinct kinetics. (**A-B**) Representative kymographs (**A**) and montages (**B**) from live TIRF microscopy of cells frown on flat and nanoridge substrates showing canonical pattern of AP2/dynamin2 fluorescence marking productive CCPs. (**C**) Lifetimes of CCPs as a function of curvature (Mean ± interquartile range, $n > 1000$ tracks from 4 cells per condition, *P*-values from Student's t test). (**D**) CCP displacement in the final 10 seconds of an endocytic site lifetime as a function of curvature (Mean ± interquartile range, $n > 1000$ tracks from 4 cells per condition, *U*-value from Mann-Whitney test). (**E**) Average normalized fluorescence intensity traces of AP2/dynamin2 for valid tracks from flat and nanoridge CCPs, binned according to lifetime. (**F**) Thin-section TEM of cells on nanoridge substrates with arrows marking coat protein atop ridge (left panel) and CCPs budding from sides of nanoridges (scale bar 100nm).

bioRxiv preprint doi: https://doi.org/10.1101/2021.07.15.452420; this version posted August 2, 2021. The copyright holder for this preprint (which was not certified by peer review) is the author/funder, who has granted bioRxiv a license to display the preprint in perpetuity. It is made available under aCC-BY-NC-ND 4.0 International license.

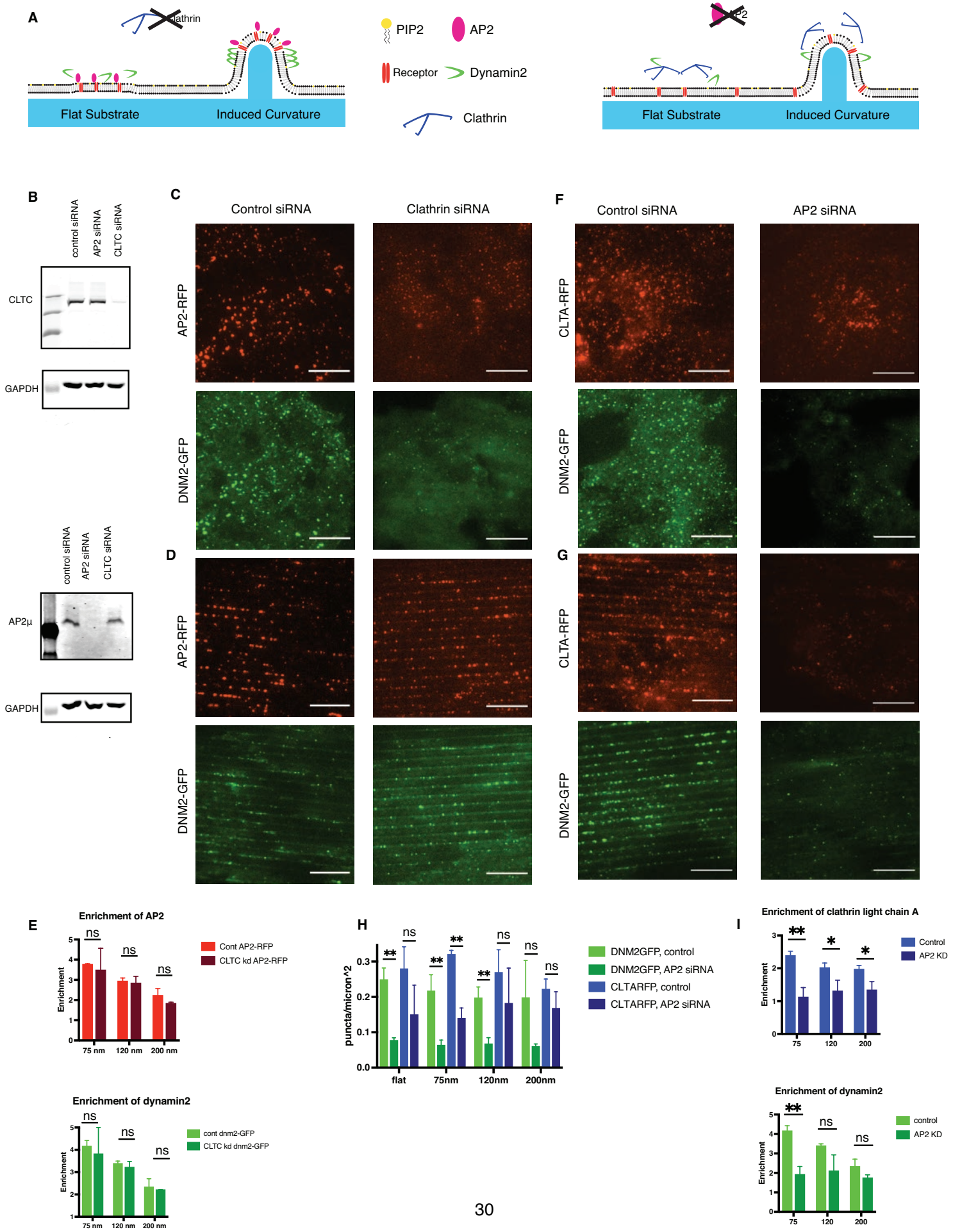

bioRxiv preprint doi: https://doi.org/10.1101/2021.07.15.452420; this version posted August 2, 2021. The copyright holder for this preprint (which was not certified by peer review) is the author/funder, who has granted bioRxiv a license to display the preprint in perpetuity. It is made available under aCC-BY-NC-ND 4.0 International license.

Fig. 4. Induced curvature rescues the localization of CCPs after clathrin knockdown but not AP2 knockdown. (**A**) Models of endocytic protein localization to flat or curved substrate with clathrin (left) or AP2 (right) disruption. (**B**) Western blots demonstrating depletion of clathrin heavy chain (top) or AP2μ subunit (bottom) 72 hours after transfection with siRNA. GAPDH was probed as a loading control. (**C**) Appearance of AP2/dnm2 proteins on flat substrate after clathrin knockdown imaged by TIRF microscopy. (**D**) Rescue of AP2 fluorescence intensity and dnm2 overlap for cells exposed to 75 nm induced curvature, imaged by TIRF microscopy. (**E**) Quantification of enrichment of AP2/dynamin2 on sites of curvature with control or clathrin siRNA (Mean ± SD, n = 3 cells per condition, P Student's t test). (**F**) Appearance of clathrin light chain-RFP and dynamin2-GFP upon AP2 knockdown and growth on flat substrate and (**G**) on 75nm induced curvature, imaged by TIRF microscopy. (**H**) Quantification of dynamin2 and clathrin light-chain A puncta with control or AP2 siRNA (Mean ±SD, n = 3 cells per condition, P Student's t test). (**I**) enrichment of remaining clathrin light chain A and dynamin2 puncta upon AP2 depletion (Mean ± SD, n = 3 conditions per cell, P Student's t test).

bioRxiv preprint doi: https://doi.org/10.1101/2021.07.15.452420; this version posted August 2, 2021. The copyright holder for this preprint (which was not certified by peer review) is the author/funder, who has granted bioRxiv a license to display the preprint in perpetuity. It is made available under aCC-BY-NC-ND 4.0 International license.

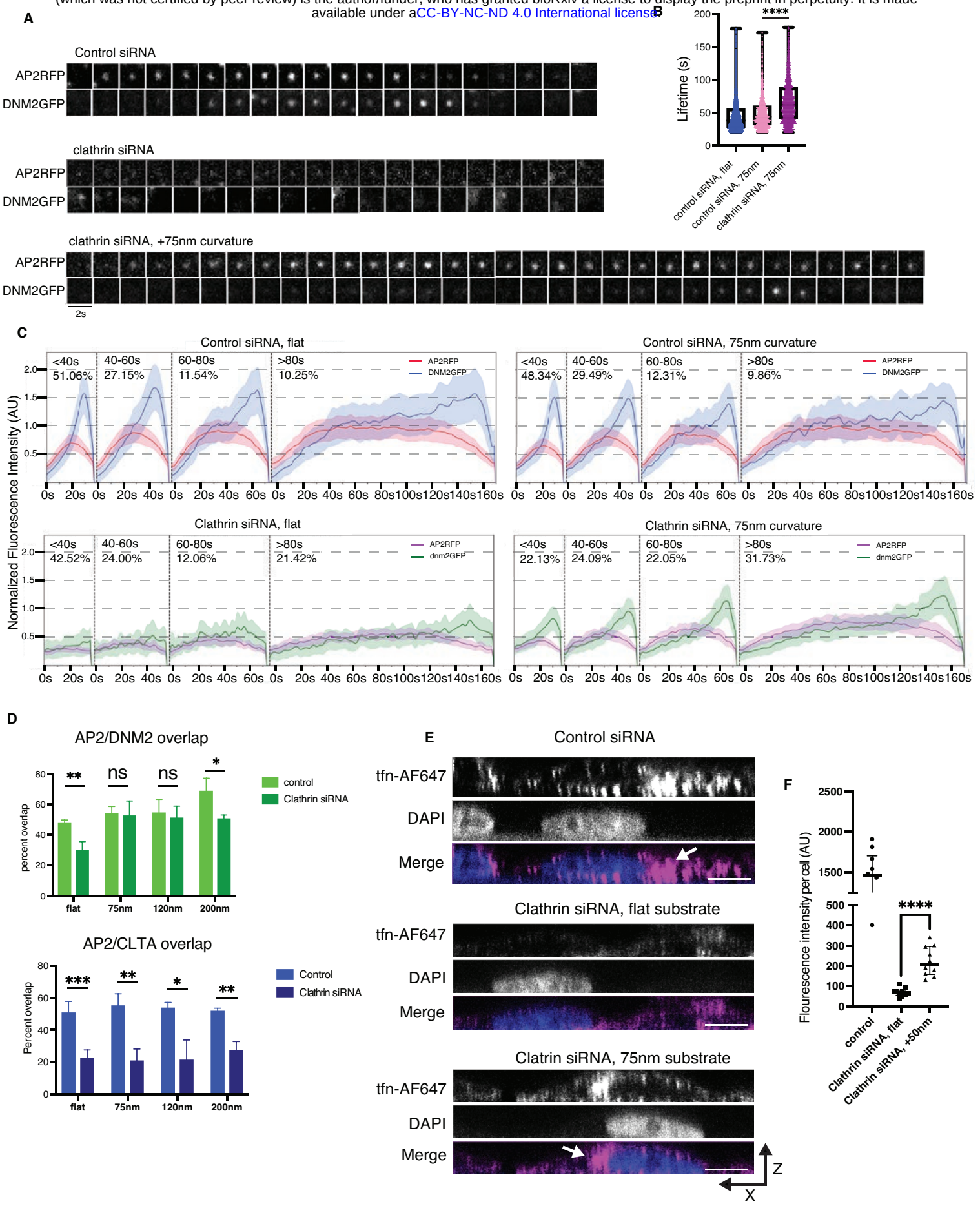

bioRxiv preprint doi: https://doi.org/10.1101/2021.07.15.452420; this version posted August 2, 2021. The copyright holder for this preprint (which was not certified by peer review) is the author/funder, who has granted bioRxiv a license to display the preprint in perpetuity. It is made available under aCC-BY-NC-ND 4.0 International license.

Fig. 5. Curvature-rescued CCPs demonstrate turnover and increased transferrin uptake. (**A**) Representative montages of detected AP2/dynamin2 events from control and clathrin knockdown cells demonstrating rescue of canonical AP2/dynamin2 turnover even after clathrin knockdown with curvature. (**B**) Lifetimes of endocytic sites from control and clathrin siRNA CCPs. (Mean ± interquartile range, $n > 1000$ tracks per condition from 3-4 cells per condition P Student's t test). (**C**) Normalized fluorescence intensity of AP2/dynamin2 CCPs from flat (left) and 75-nm curvature (right) with control or clathrin siRNA. (**D**) Detected overlap of AP2/ dynamin2 or AP2/clathrin light chain upon clathrin heavy chain knockdown (Mean ± SD, $n = 3$ cells per condition, p Student's t test). (**E**) X-Z reconstructions of slices through the middle of cells after transferrin uptake assays from confocal microscopy of control siRNA and clathrin siRNA, with white arrows indicating perinuclear transferrin (scale bar 10 μM). (**F**) Quantification of transferrin fluorescence intensity per cell of clathrin siRNA-treated cells with or without induced curvature (Mean ± SD, $P < 0.0001$ Student's t test).